Tunable Fabry-Pérot Filter for Optical Glucose Monitoring

Xin Zhao[1,2] and Schmidt J. Dominik[2]
[1]College of Physical Science and Technology, Sichuan University, 29 Wangjiang Road, Chengdu, Sichuan, P.R. China,
[2]Department of Electrical Engineering, International Technological University,
355W San Fernando St, San Jose, CA, U.S.A.

Keywords: Micro-electro-mechanical Systems, Long-Wave Infrared, Tunable Fabry-Pérot Filter, Glucose Sensor.

Abstract: This paper presents a Tunable MEMS Fabry-Pérot (FP) filter for the application of optical glucose sensor in Long-Wave Infrared (LWIR) range. The structure design, simulation, fabrication process and testing system are reported. The spectral wavelength tuning range from 10.9 μm to 12.19 μm was designed for the transmission peak which is related to the glucose concentration. A tuning distance between top and bottom reflector of 2.25μm has been achieved, while maintaining a relatively low tuning voltage of 20V. The Tunable FP filter is the core part of glucose sensor and has other applications in Bio-sensor, hyperspectral imaging and tunable lasers, etc.

1 INTRODUCTION

Blood Glucose monitoring technologies have been used in the treatment of diabetes for three decades. The invasive methods are based on microneedle, impedance spectroscopy, microdialysis and subcutaneous sensor, etc. The developing non-invasive sensors use infrared absorption, optical coherence tomography, Raman scattering, and polarimetry as measurement technologies.

Recently, infrared spectroscopy has shown the potential for an analytical method in non-invasive glucose sensing based on the optical characteristic of the glucose concentration. On the other hand, with the development of micromachining technologies, Micro-electro-mechanical Systems (MEMS) emerges as the choice for the fabrication of Infrared (IR) instrument. Compared with conventional IR analysis systems, the MEMS IR sensors offer lower cost, lower power consumption and more portability due to their small size.

As the key part of optical non-invasive glucose sensor, the tunable MEMS FP filter was originally developed by several different groups. Noro's group reported the 3-5 μm Mid-wave Infrared (MWIR) filter for the gas sensing. Stupar's group presented the first LWIR tunable filter range from 8 μm to 11 μm. The dual-band FP filter with two reflectors was reported by Neumann's group. The spectral ranges are from 4 μm to 5 μm and from 8 μm to 10.5 μm.

In this paper, a tunable MEMS FP filter for the LWIR range is presented. The proposed bulk micromaching technology is used to form the reflector carriers. The tunable FP filter could be combined with a detector to test the central wavelength shift of transmission peak which can read out the change of glucose concentration in the human body.

2 DESIGN OF TUNABLE FP FILTER

2.1 MEMS Design

Figure 1(a) shows the structure of the tunable FP filter, which consists of two 2.1× 2.1 mm² reflectors, two 3.6 × 3.6 mm² reflector carriers, and four springs. The bottom reflector carrier is fixed and the other suspended by springs. The reflectors are surrounded by a metal electrode which uses an electrostatic force between the two reflector carriers to change the distance between the reflectors as shown in Fig. 1(b). The L shaped springs are applied on the structure design to optimize the the flatness across the central area of the top reflector.

Zhao X. and J. Dominik S..
Tunable Fabry-Pérot Filter for Optical Glucose Monitoring.
DOI: 10.5220/0004871101710175
In *Proceedings of the International Conference on Biomedical Electronics and Devices* (BIODEVICES-2014), pages 171-175
ISBN: 978-989-758-013-0

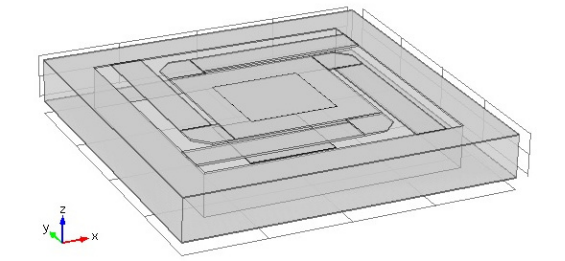

(a)

(b)

Figure 1(a): Schematic of the tunable FP filter, (b) cross-section of the tunable FP filter.

2.2 Optical System

The electromagnetic waves enter the optical cavity through the top reflector and are reflected by both the top and bottom reflector many times. The output transmittance spectrum $T(\lambda)$ of the FP filter is described by the Airy-Function

$$T(\lambda) = T_{pk}[1 + \frac{4R}{(1-R)^2}\sin^2(\delta)]^{-1} \quad (1)$$

with the optical phase

$$\delta(\lambda) = \frac{2\pi n d \cos\theta}{\lambda} - \phi(\lambda) \quad (2)$$

and the peak transmittance

$$T_{pk} = \left(1 - \frac{A}{1-R}\right)^2 \quad (3)$$

Where λ is the wavelength of the electromagnetic, R is the reflectance, n is the refractive index of the material between the reflectors, d is the distance between the top and bottom reflector, θ is the angle of incidence, ϕ is phase shift on reflection, and A is the absorption as shown in Fig.2.

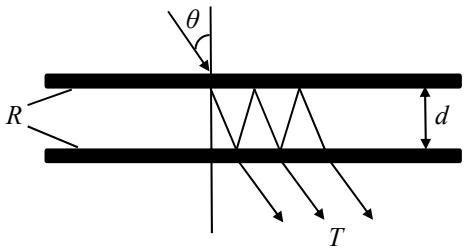

Figure 2: Schematic of Fabry-Pérot filter.

The reflectors are distributed Bragg reflector (DBR) mirrors which contain Ge/Al_2O_3/Ge layers. The thickness of the Ge layers and Al_2O_3 layer are 850 nm and 629 nm, respectively. The electrical field distribution of DBR is related to the peak value of the transmission. The simulation result of the 3D electrical field distribution of the DBR is shown in Fig. 3. The optical properties simulation is performed by software COMSOL by using finite element methods.

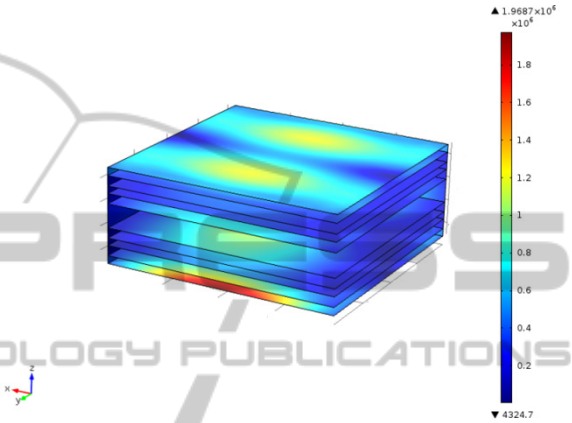

Figure 3: The 3D electrical field distribution.

The central wavelength (CWL) of the output transmission peak is related to the distance between the top and bottom reflector. As shown in Fig. 4, The CWL is 11.56 μm, when the distance between the top and bottom reflector is 6.17 μm.

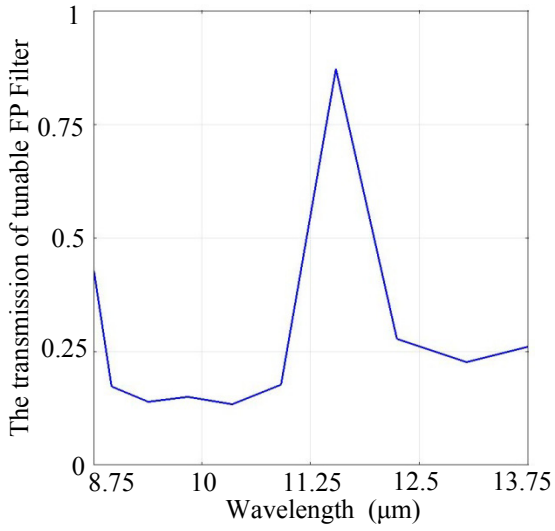

Figure 4: The simulated transmission of the tunable FP filter.

2.3 Electromechanical System

The metal layers in top and bottom reflector carriers consist of capacitor structure. The electrostatic force of the capacitor results in the change of the distance between the top and bottom reflector when the voltage is applied on the planes of capacitor.
The electrical force F of the capacitor structure can be expressed by

$$F = \frac{CV^2}{2d} \quad (4)$$

Where C is the capacitance, V is the voltage between the two planes. The bottom of the plane is fixed, therefore, the pressure P on the top plane is

$$P = \frac{CV^2}{2Sd} \quad (5)$$

Where S is the area of the capacitor plane. The electromechanical simulation is performed by the software COMSOL. The C is 11.1763 pf, when the voltage is 20 V, S is 8.55 mm^2 and d is 6.8 μm. The displacement of the top reflector is 2.25 μm as shown in the Fig. 5, when the voltage on the top plane is 20 V. Because the bottom reflector is fixed, the displacement of the top reflector is equal to the change of distance between the top and bottom reflector.

When the voltage changes from 0 V to 20 V, the distance between the top and bottom reflector plates increases from 0 μm to 2.25 μm as shown in the Fig. 6. Due to the pull-in effect, the tuning distance between the two reflectors should be less than 2.27 μm which is one third of the initial distance 6.8 μm. In order to get the stable tuning range of the transmission, the input voltage should be less than 20V.

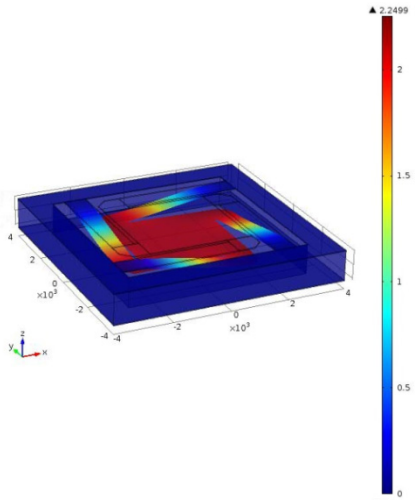

Figure 5: The displacement of the top reflector.

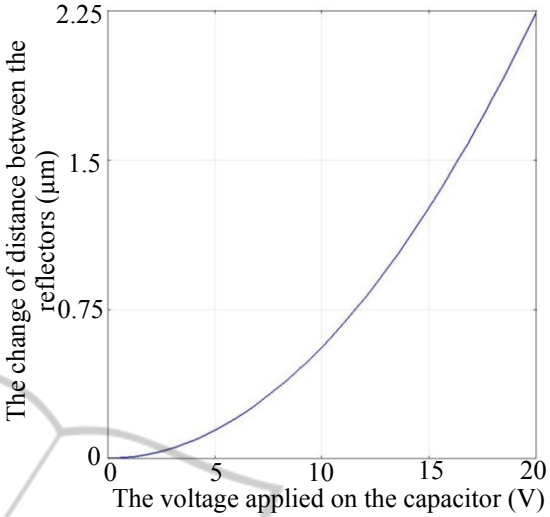

Figure 6: The change of distance between the top and bottom reflector due to the applied voltage.

The change of distance between the top and bottom reflector results in the transmission peak shift, when the voltage is different as shown in Fig. 7. When the voltages are 0 V, 14 V and 20V, the central wavelength of the transmission peaks are 12.19 μm, 11.56 μm, and 10.9 μm, respectively. As shown in the Fig. 8, when the voltage changes from 0V to 20 V, the transmission peak shift increases from 0 μm to 1.29 μm.

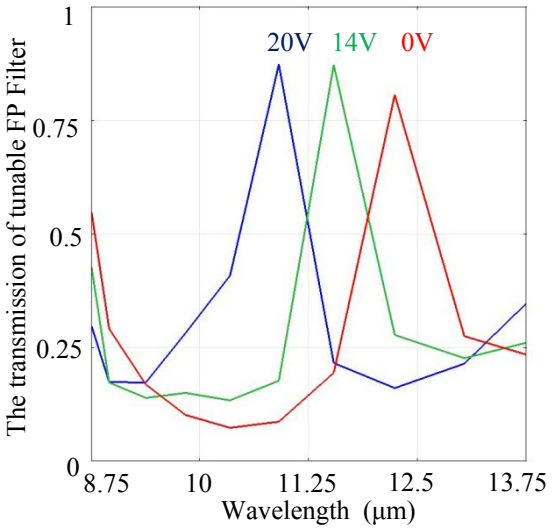

Figure 7: The transmission peak of the tunable FP filter.

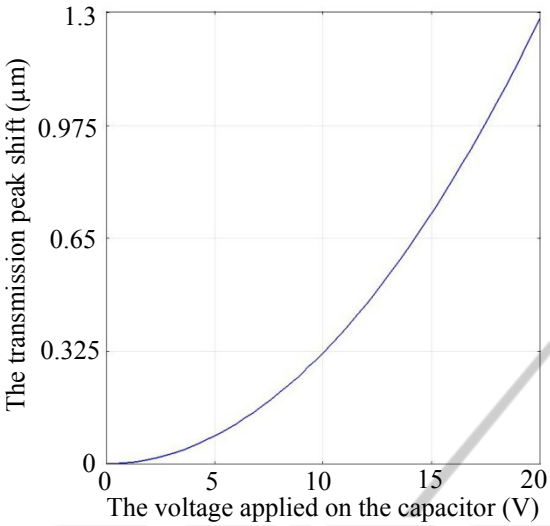

Figure 8: The transmission peak shift due to the applied voltage on the capacitor.

2.4 Fabrication

The proposed fabrication of the MEMS Fabry-Pérot filter is based on a bulk micromachining approach. Two structured wafers are bonded together by an intermediate SU8-layer to form the top and bottom reflector. The optical area in the center of the chip is surrounded by control electrodes.

The silicon wafer is 4 inch in diameter and 525 µm thick. In order to achieve good transmittivity, the wafer is polished to reduce the thickness to 300 µm. The fabrication starts with deposition of silicon dioxide which is used as the block layer of wet etching of silicon as shown in Fig. 9(a).

The silicon dioxide layer is under etching by buffered oxide etch (BOE) to form the window for silicon etching as shown in Fig. 9(b). The silicon is selectively etched by Tetramethylammoniµm hydroxide (TMAH) from backside as shown in Fig. 9(c).

In the next step, the other silicon dioxide is etched by BOE as shown in Fig. 9(d), and the springs of the top movable reflector carrier is formed by etching the silicon material as shown in Fig. 9(e). The proposed DBR structure of the reflector is formed by depositing Ge/Al_2O_3/Ge layers as shown in Fig. 9(f). The thickness of the Ge layers of is 850 nm and the thickness of the Al2O3 layer is 629 nm. Germanium Evaporation is realized by Innotec ES26C E-Gun Evaporator. Al_2O_3 deposition is fabricated by the plasma-enabled atomic layer deposition (ALD) system.

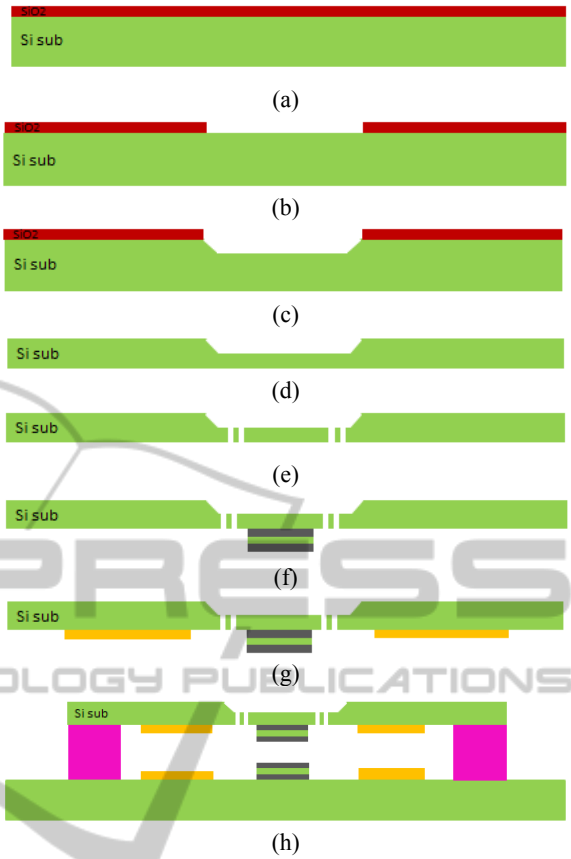

Figure 9(a)-(h): The fabrication process flow of the tunable FP filter.

The top electrode is formed by using physical vapour deposition Sputter System to sputter Au in the front side of substrate as shown in Fig. 9(g). The thickness of the Au layer is 0.5 µm.

The fabrication of the bottom reflector carrier is similar to the top reflector carrier except for the etching process to form the backside open and springs. Both the wafers with the movable top and the bottom fixed reflector carriers respectively are connected with a SU-8 interface layer as shown in Fig. 9(h).

The proposed layout of the tunable FP filter is shown in Fig. 10. Ledit software is used to draw the layout. The width of the reflector is 2.1mm. The width of the spring is 0.75 mm and the movable area of the top carrier is 3.6 × 3.6 mm. The area of the metal pad is 1.2 × 1.2 mm.

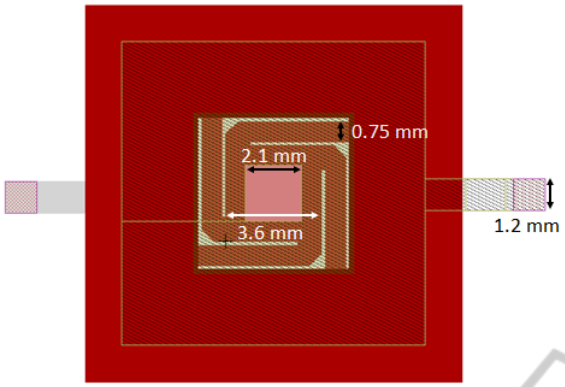

Figure 10: The layout of the tunable FP filter.

2.5 Testing System

In order to control the voltage between the top and bottom capacitor planes, a Korad voltage supply KA6003P can be used as reference. The voltage supply is a programmable single-channel, constant-voltage power supply with low noise, high reliability and high accuracy.

The glucose sensor system consists of a voltage supply, tunable FP filter, detector, testing circuit, and PC as shown in Fig. 11. The reference detector is a thermopile detector MLX90614 from Melexis. The MLX90614 is an Infrared thermometer for non-contact temperature measurements. Both the IR sensitive thermopile detector chip and the signal conditioning ASIC are integrated in the same TO-39 can. Evaluation board EVB90614 from Melexis is used as the testing circuit which includes an easy interface between the MLX90614 infrared thermometer in TO-can and a PC.

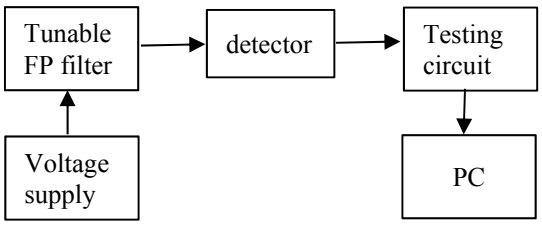

Figure 11: The schematic of glucose sensor system.

3 CONCLUSIONS

In summary, a tunable MEMS Fabry-Pérot filter for the Long-Wave Infrared range is proposed and simulated. By applying a voltage ranging from 0 V to 20 V, the tuning range of output transmission peak shift from 10.9 μm to 12.19 μm is obtained. The tunable FP filter is the key part of glucose sensor and has other applications in hyperspectral imaging, spectrometers, telecommunication and light sources, etc.

REFERENCES

Smart WH, Subramanian K., 2000. The use of silicon microfabrication technology in painless blood glucose monitoring. *Diabetes Technol Ther*.

Pfützner A, Caduff A, Larbig M, Schrepfer T, Forst T., 2004. Impact of posture and fixation technique on impedance spectroscopy used for continuous and non-invasive glucose monitoring. *Diabetes Technol Ther* .

Rossetti P, Porecellati F, Fanelli CG, Bolli GB., 2006. Evaluation of the accuracy of a microdialysis-based glucose sensor during insulin-induced hypoglycaemia, its recovery, and post-hypoglycaemic hyperglycaemia in humans. *Diabetes Technol Ther.*

Cass AEG, Francis DG, Hill HAO, Aston WJ, Higgins IJ, Plotkin EV., 1984. Ferrocene-mediated enzyme electrode for the amperometric determination of glucose. *Anal Chem*.

Shen YC, Davies AG, Linfield EH, Taday PF, Arnone DD., 2003 The use of Fournier-transform infrared spectroscopy for the quantitative determination of glucose concentration in whole blood. *Phys Med Biol.*

Esenaliev RO, Larin KV, Larina IV., 2001 Non-invasive monitoring of glucose concentration with optical coherence tomography. *Optics Letter.*

Dieringer JA, McFarland AD, Shah NC, Stuart DA, Whitney AV,Yonzon CR., 2006. Surface-enhanced Raman spectroscopy: new materials, concepts, characterization tools, and applications. *Faraday Discuss.*

Cameron BD, Baba JS, Coté GL., 2001. Measurement of the glucose transport time delay between the blood and aqueous humour of the eye for the eventual development of a non-invasive glucose sensor. *Diabetes Technol Ther* .

Malchoff CD, Shoukri K, Landau JI, Buchert JM., 2002. A novel non-invasive blood glucose monitor. *Diabetes Care.*

Noro, M., Suzuki, K., Kishi, N., Hara, H.,Watanabe, T., Iwaoko, H., 2003. CO2/H2O gas sensor using tunable Fabry-Pérot filter with wide wavelength range. *Proc. IEEE MEMS 2003 Conf.*

Stupar, P. A., Borwick, R. L., DeNatale, J. F., Kobrin, P. H., Gunning, W. J., 2009. MEMS tunable Fabry-Pérot filters with thick, two sided optical coatings. *Proc. IEEE Transducers 2009 Conf.*

N. Neumann, M. Ebermann, E. Gittler, M. Meinig, S. Kurth, and K. Hiller., 2010. Uncooled IR sensors with tunable MEMS Fabry-Pérot filters for the long-wave infrared range. In *Sensors, 2010 IEEE.*

Macleod, H.A., 2001. Thin-Film optical filters, IoP, Bristol and Philadelphia.